Capacitive behavior of pentacene-based diodes: Quasistatic dielectric constant and dielectric strength

Chang Hyun Kim, Omid Yaghmazadeh, Denis Tondelier, Yong Bin Jeong, Yvan Bonnassieux, Gilles Horowitz

Capacitive behavior of pentacene-based diodes: Quasistatic dielectric constant and dielectric strength

Chang Hyun Kim,[a] Omid Yaghmazadeh, Denis Tondelier, Yong Bin Jeong, Yvan Bonnassieux, and Gilles Horowitz[b]
LPICM, Ecole Polytechnique, CNRS, 91128 Palaiseau Cedex, France

(Received 15 December 2010; accepted 10 March 2011; published online 20 April 2011)

The capacitive behavior of pentacene films was investigated in the metal-semiconductor-metal (MSM) diode structure. Impedance analysis of diodes with a thick pentacene layer up to 1012 nm showed a full depletion of the organic layer. This observation allowed us to regard the MSM diode as a parallel-plate capacitor in the reverse-bias regime without current flow. Under forward-bias, the diode was evaluated through frequency-dependent impedance measurements by using an equivalent circuit composed of a single parallel resistance-capacitance circuit. The analysis of the data in both the reverse and forward bias regime led us to electrical methods for quantifying dielectric properties of pentacene. © *2011 American Institute of Physics*. [doi:10.1063/1.3574661]

I. INTRODUCTION

The development of organic electronic devices stems from the continuous interest in low-cost, flexible electronic products. Organic light-emitting diodes (OLEDs), organic thin-film transistors (OTFTs), and organic photovoltaic cells (OPVs) are the most widely studied devices in both academic and industrial laboratories. In spite of remarkable progress in their performance, the fundamental physics on organic devices is still lacking, and many physical topics remain controversial. As an example, two recent articles[1,2] on the current−voltage characteristics of organic diodes using rubrene single crystals explain similar experimental data with totally different concepts. Kaji *et al*. described the metal-semiconductor contact as a Schottky contact based on the formation and modulation of a depletion region near the contact.[1] The theory of Schottky diode is often adopted for describing devices based on metal/organic contacts.[3–5] Braga *et al*., however, used impedance analysis to bring evidence for that there is no modulation of a depletion region. Instead, the organic layer is always fully depleted due to the very low carrier density in highly pure organic semiconductor.

The classical Schottky diode theory predicts voltage-controlled depletion capacitance under reverse-bias. This is due to the modulation of the depletion width at the rectifying contact and the analysis of $1/C^2-V$ plot is a well-known technique to extract the built-in potential and the doping concentration of the semiconductor.[6] By contrast, a fully depleted organic semiconductor shows a voltage-independent, constant reverse-bias capacitance.

Our work starts with this highly controversial argument on the formation of a depletion region in organic semiconductor by systematically characterizing organic diodes made of pentacene, one of the most widely used organic semiconductor. Impedance measurements led us to confirm the full depletion of this organic semiconductor, as the reverse-bias data correspond to a pure, voltage-independent capacitance. Considering the pentacene diode as a pure capacitor, we could extract the quasistatic dielectric constant and the dielectric strength of pentacene.

In terms of practical application, high-performance organic diode was suggested with confidence as a rectifying device in organic radio-frequency identification (RF-ID) tags.[7,8] Furthermore, we believe that the implications found in this study can serve as an important element for understanding any kinds of organic electronic devices which should possess several metal/organic contacts.

II. EXPERIMENTAL

Pentacene-based organic diodes were fabricated with the Au/pentacene/Al structure (inset of Fig. 1). Ten nanometers of Al was first deposited by vacuum evaporation on a glass substrate as an adhesion layer and 50 nm of Au (bottom electrode) was evaporated next. Pentacene (Sigma Aldrich, 99.9+ % purity, used without further purification) was then thermally evaporated to form relatively thick semiconducting films. In this report, two sets of devices are dealt with in order to investigate the effect of semiconductor thickness on the analysis. Set A has a pentacene layer of ~530 nm (average thickness) and Set B of ~1052 nm. Each set of device contains few tens of diodes with four different active areas (overlap region of top and bottom electrodes); 4.3×10^{-4} cm^2, 9.5×10^{-4} cm^2, 2.3×10^{-3} cm^2, and 3.8×10^{-3} cm^2. For Set A, 80 nm of Al (top electrode) was finally evaporated and 150 nm of Al for Set B.

The process parameters for both sets of devices were carefully controlled to be as similar as possible. All evaporation processes were done under a pressure of about 2×10^{-7} mbar and the substrate was kept at room temperature (24 °C). The evaporation rate of pentacene was kept at 0.1 nm/s. The evaporation system is setup in a nitrogen-filled glovebox and all layers are subsequently deposited in the same chamber with minimum time interval to avoid any contamination or degradation. The final samples were transferred into another

[a]Electronic mail: chang-hyun.kim@polytechnique.edu.
[b]On leave from ITODYS, Université Paris Diderot, 75205 Paris, France.

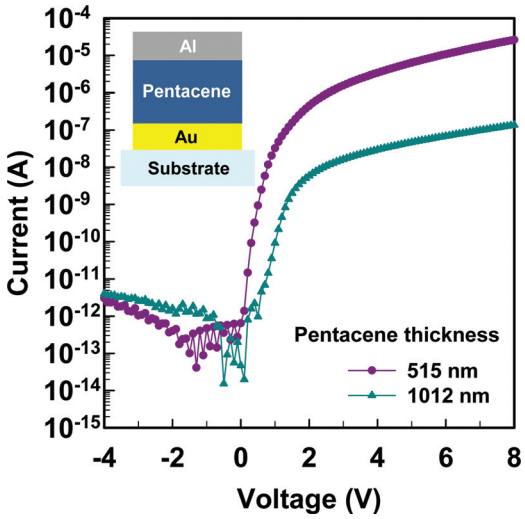

FIG. 1. (Color online) Representative $I-V$ characteristics of pentacene-based organic diodes. The inset illustrates the diode structure with Au/pentacene/Al on a glass substrate.

glove box equipped with the electrical measurement system. This procedure allowed us to fabricate and analyze the samples without any exposure to the ambient air. Current−voltage ($I-V$) measurements were carried out using a semiconductor characterization system (Keithley 4200) and impedance measurements were conducted using a HP 4192A LF impedance analyzer. The thickness of the pentacene layer at different points (individual diodes) was precisely determined with a surface profiler (Dektak 150 surface profiler, Veeco). Tapping-mode atomic force microscopy (AFM) images of pentacene were taken using Veeco Dimension 5000 AFM system. All electrical measurements were done in the dark at room temperature, and performed right after the fabrication process.

III. RESULTS AND DISCUSSION

A. Current−voltage curves

Figure 1 shows representative $I-V$ curves of the pentacene diodes (a diode with 515 nm of pentacene from Set A and another diode with 1012 nm of pentacene from Set B). The active area of both diodes is 4.3×10^{-4}cm^2. The applied voltage (V_a) corresponds to the voltage at the Au electrode (anode) with the Al electrode (cathode) grounded. Measured currents in the reverse-bias regime ($V_a < 0$ V) are always extremely low, near the detection limit of the measurement system, due to the low leakage current injection from the Al contact. In the forward-bias regime ($V_a > 0$ V), the current increases sharply due to the injected holes from Au electrode. A detailed physical description of the $I-V$ characteristics will be discussed with the proposed energy diagrams in Sec. III C. The rectification ratio is as high as $\sim 10^6$ (515 nm sample) and $\sim 10^4$ (1012 nm sample) even within a low voltage range of ± 2 V. These values very favorably compare to other works on organic diodes.[2,7,9,10] The inset in Fig. 1 is a schematic view of the metal-semiconductor-metal (MSM) structure of the diode.

$I-V$ characteristics presented in Fig. 1 look very similar to those of Schottky diodes and this is the reason why the classical Schottky theory is frequently employed for the analysis of metal/organic rectifying contact. Based on the very low carrier density in unintentionally doped organic semiconductors, however, we could prove by means of impedance−voltage ($Z-V$) measurements that thick films of pentacene up to 1012 nm are "fully" depleted (even at thermal equilibrium with $V_a = 0$ V). Accordingly, we argue that the general picture of metal/organic interfaces does not contain any "partial" depletion region and the resulting band bending at the interface. Note that we purposely chose very thick layers of pentacene to make sure that organic diodes in practical application with a thickness of the order of 100 nm or less cannot possibly bear the formation of a depletion region.

B. Impedance measurements in the reverse-bias regime

Figure 2 shows $Z-V$ characteristics of two representative diodes from each set (device area: 4.3×10^{-4} cm^2). Figure 2(a) is the measured $Z-V$ curve of the 515-nm diode and Fig. 2(b) is the result of the 1012-nm diode. The small-signal ac frequency is fixed as 50 kHz for both measurements.

Two operation regimes (reverse and forward) are clearly distinguishable in Fig. 2. When the organic diode is reverse-

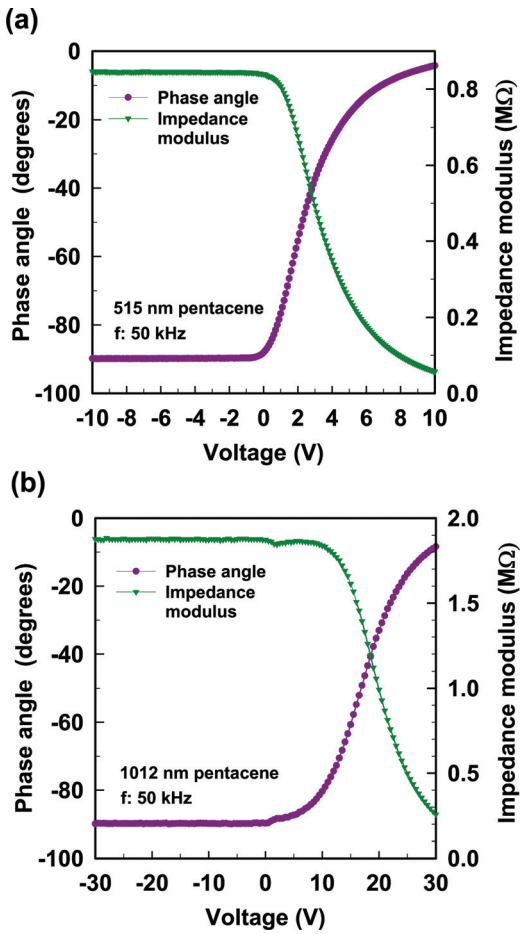

FIG. 2. (Color online) Impedance-voltage ($Z-V$) data showing fully depleted organic layer in the reverse-bias regime. The active area of both diodes is 4.3×10^{-4} cm^2. (a) $Z-V$ characteristics of the diode with 515 nm of pentacene. (b) $Z-V$ characteristics of the diode with 1012 nm of pentacene.

biased ($V_a < 0$ V), the phase angle is always $-90°$ and the modulus is constant, which clearly indicates that the diode behaves as a pure capacitance, meaning that the pentacene layer is fully depleted. Such a behavior is often encountered in organic thin-film diodes, as for instance in OLEDs that typically contain organic layers a few tens of nanometers thick, where they are most likely described as fully depleted.[11] The observed full depletion of 515- and 1012-nm-thick pentacene films is a consequence of the extremely low doping density in unintentionally doped organic semiconductors.[12] Note that if there existed a space charge layer at the rectifying pentacene/Al contact with a depletion width less than the semiconductor thickness, we would observe a voltage-dependent impedance modulus (or capacitance). In the forward-bias regime ($V_a > 0$ V), the diode is no longer purely capacitive (phase angle approaching 0°) but a capacitance can still be estimated as will be discussed in Sec. III D.

The impedance (Z) of a circuit is defined as the ratio of the phasor voltage and the phasor current measured in ohms (Ω).[13] As the equivalent circuit of pentacene diodes in the reverse-bias regime is a single constant capacitor, the impedance should be expressed as

$$Z = \frac{1}{j\omega C}, \tag{1}$$

where j is the imaginary unit, ω the (angular) frequency of the applied ac small-signal, and C the capacitance. As Z is a complex number, its modulus and phase angle could be separately analyzed as shown in Fig. 2. We note that the impedance modulus is so high under reverse-bias (MΩ order) that the applied ac frequency should be set high enough. In other words, according to Eq. (1), at frequencies lower than 50 kHz the modulus falls out of the detection limit of our measurement instrument. We could test some diodes with larger areas which could be measured at lower frequency (down to 10 kHz) and the full depletion was always observed regardless of the frequency. Furthermore, we will show in Secs. III D and III E that there is no frequency dependence of the capacitive properties over a broad frequency range.

If we assume uniform-doping profile in the semiconductor, the depletion width W is determined by equation

$$W = \sqrt{\frac{2\varepsilon_s(V_{\rm bi} - V_a)}{qN_a}}, \tag{2}$$

where ε_s is the permittivity of the semiconductor, $V_{\rm bi}$ the built-in potential of the diodes (equivalent to the diffusion potential in Sec. III C), V_a the applied anode voltage, q the elementary charge, and N_a the doping concentration.[6] Experimentally proved full depletion of up to 1012 nm of pentacene enables the calculation of the upper limit of the doping concentration in the pentacene layer.

With the extracted quasistatic dielectric constant of pentacene in Sec. III E (average value of 3.61) and the built-in potential of 0.7 V, calculation of N_a from Eq. (2) reveals that the (unintentional) doping concentration of pentacene is lower than 2.7×10^{14} cm^{-3}. In most practical applications, "thin-film" diodes or transistors for example, the deposited organic semiconducting layers are around 100 nm thick or thinner. Calculated from Eq. (2), 100 nm pentacene films are fully depleted even if N_a is raised up to 2.8×10^{16} cm^{-3}. In general, it is not straightforward to determine the exact doping concentration of organic semiconductors; however, some works provide estimations of several unintentionally doped semiconductors including rubrene single crystal,[14] thiophene oligomer,[15] and poly(3-hexylthiophene) (P3HT).[16] The suggested doping concentrations are of the order of 10^{11} to 10^{16} cm^{-3}, which fall into the full depletion range for a 100 nm thick organic film (the dielectric constant and built-in potential evidently depend on the given devices but they do not significantly vary in most cases).

The proof of full depletion in 1000 nm thick pentacene layers points out the extremely low doping concentration of pentacene (less than 10^{14} cm^{-3}), and it is worth mentioning that most of undoped or unintentionally doped organic semiconductors should be depicted as fully depleted as long as films with moderate thickness are under scrutiny.

C. Metal-insulator-metal (MIM) model

From the clear evidence for full depletion, the utilization of the metal-insulator-metal (MIM) model for organic diode

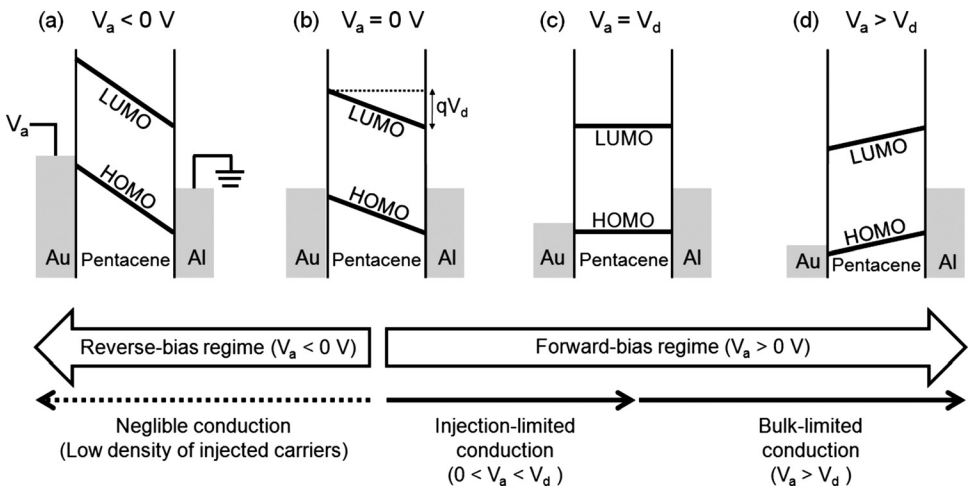

FIG. 3. MIM type energy diagram of a pentacene diode at different operation regimes. (a) Reverse-bias regime, (b) thermal equilibrium, (c) flat-band condition, (d) bulk-limited forward-bias regime. The lower panel indicates the dominant conduction mechanisms under each bias regime.

is suggested in Fig. 3. This picture differs totally from the Schottky-type band diagram with band bending at the interface that was previously proposed for a similar pentacene diode.[10] Referenced energy levels for drawing this diagram are as follows; the work function of Au as 4.9 eV, the work function of Al as 4.2 eV, the ionization potential of pentacene as 5.2 eV, and the electron affinity of pentacene as 2.8 eV.[2,10,17,18] V_d is defined as the diffusion (or built-in) potential, which originates from the difference between the work functions of the two contact metals; the Au/Al pair gives a V_d of 0.7 eV. Taking into consideration the injection energy barriers, we can assume that the LUMO level of pentacene is sufficiently far from the Fermi levels of both Au and Al so that electron injection from either electrode into the LUMO level of pentacene can be neglected and single-carrier conduction takes place (hole-only conduction). Another hypothesis is that injection of holes from Al into the HOMO level of pentacene is also negligible due to the high injection barrier of about 1 eV. In contrast, Au electrode has a very low injection barrier of 0.3 eV into the HOMO level of pentacene so that it can supply high density of injected holes. Making use of these specificities, we can call the Au electrode the (hole-) "injecting electrode" while the Al electrode should be mentioned as the "blocking electrode" (for both types of carriers).

At thermal equilibrium [Fig. 3(b)], Fermi level alignment of the two electrodes takes place. Fermi level alignment normally causes the formation of band bending and the depletion width is dependent on the Fermi-level difference and the doping density [Eq. (2)]. There could be a formation of the depletion region at the Al/pentacene interface due to the large Fermi-level mismatch. Nevertheless, when the doping concentration is extremely low, the depletion width exceeds the whole thickness of the semiconductor [Eq. (2)] and this is exactly what is proved by the $Z-V$ measurements in Fig. 2. As a result of full depletion, we can infer that the density of "thermally generated" carriers is negligible, and that the current entirely comes from "injected" carriers. HOMO and LUMO bands have linear shapes between the two electrodes like a MIM capacitor.

When the diode is reverse-biased [Fig. 3(a)], due to the negligible carrier injection from both electrodes, there is no significant current flow and the diode is a perfect capacitor (Figs. 1 and 2).

In the forward-bias regime [Figs. 3(b)–3(d)], there are two different mechanisms of conduction; the injection-limited and the bulk-limited conduction. Theoretically, for determining which mechanism is dominant, one should refer to mathematical models for each conduction mechanism.[11,19–21] When the forward-bias voltage is lower than V_d, injection of holes dominates the current. This is because there are no charge carriers in the pentacene itself. Evidence for injection-limited conduction comes from the linearity of the $I-V$ curves in semilogarithmic scales (Fig. 1) in this regime ($0\ \text{V} < V_a < V_d$); that is, the current is an exponential function of the voltage.[6,11] When the applied voltage is higher than V_d, we observe a downward bending of the $I-V$ curves. Now the injection of holes is no longer the limiting factor; rather, the current is limited by the transport of charges across the bulk of the semiconductor layer and the $I-V$ characteristic follows a power-law dependence with a scaling exponent reflecting the distribution of traps in the semiconductor.[11,21]

In order to further investigate the validity of the MIM model for organic diodes, physically based two-dimensional device simulation (ATLAS simulator by SILVACO, Inc.) was conducted. The simulation involves solving a set of coupled Poisson's, continuity and transport equations within the defined two-dimensional device structure. Important physical information such as electric field distribution, carrier concentration, potential profile can be directly accessed from the calculation. Drift-diffusion model is taken for the transport equation and the Au/pentacene/Al structure is defined to simulate the 515-nm pentacene diode.

Simulated potential profiles with a variation of the injection barrier at the Au/pentacene contact are shown in Fig. 4.

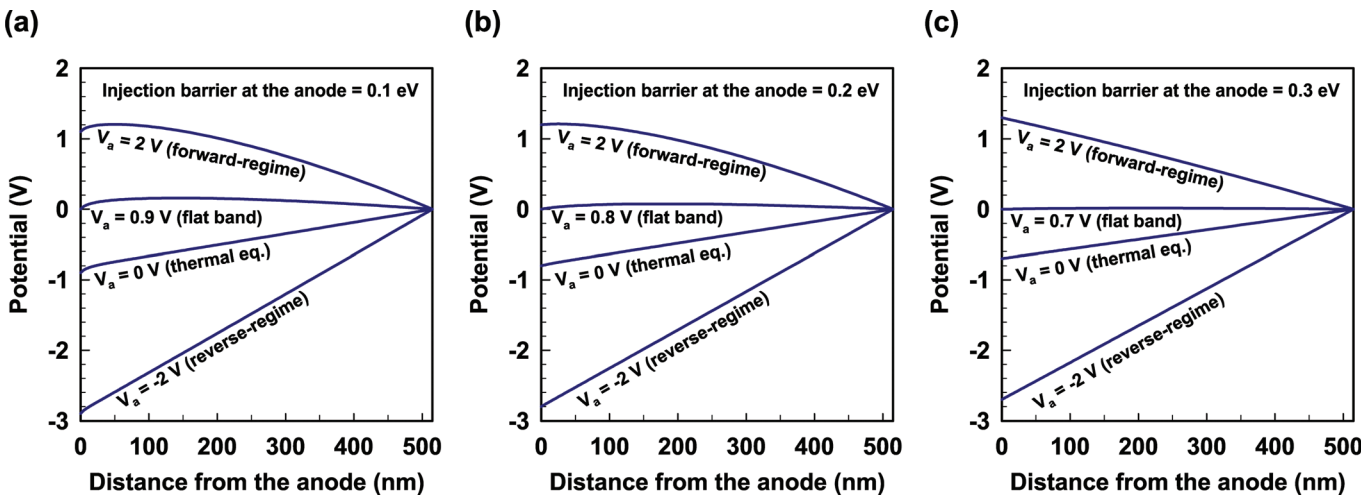

FIG. 4. (Color online) Simulated potential profiles in the 515-nm pentacene layer. The ionization potential of pentacene is 5.2 eV and the work function of the cathode (Al) is 4.2 eV in all three cases with different hole injection barrier values at the anode; (a) 0.1 eV barrier (work function of Au anode as 5.1 eV), (2) 0.2 eV barrier (work function of Au anode as 5.0 eV), (c) 0.3 eV barrier (work function of Au anode as 4.9 eV).

The reference potential (0 V) is the potential of the Al top electrode (at $x = 515$ nm). In the simulated structure, the ionization potential and the electron affinity of pentacene are set to 5.2 and 2.8 eV, respectively. The work function of Al (cathode) is fixed as 4.2 eV, while the work function of Au (anode) was varied (5.1, 5.0, and 4.9 eV) in order to emphasize the injection barrier height-dependent behavior. At this point, it is worth reminding that the hole concentration p_0 at the metal-semiconductor interface is largely controlled by the injection barrier and determined by[6]

$$p_0 = N_v \exp\left(\frac{-E_b}{kT}\right), \tag{3}$$

where N_v is the effective density of states at the valence band (HOMO) edge (assumed to be 10^{20} cm^{-3} for the simulation), E_b the hole injection barrier height, which equals the difference between the metal work function and the semiconductor ionization potential, k the Boltzmann constant, and T the absolute temperature.

Even though the MIM model seems to be correct in the reverse-bias regime (the profiles at $V_a = -2$ V) in all cases, slight band bending can be observed at the "injecting" Au contact (meaning that this cannot be a "depletion"-related band bending) for small barriers (0.1 or 0.2 eV). This band bending is more pronounced when the diode is forward-biased (the profiles with $V_a = 2$ V). From the classical injection theory, this effect is the result of a formation of the virtual anode inside the semiconductor.[21,22] When an ohmic contact is considered, this contact may act as a reservoir of carriers and the internal electric field forms (a band bending occurs) to push the injected holes back toward the metal. When a forward-bias is applied, the 'applied" electric field is compensated by the "internal" field and there exists a physical position where the field is zero (the derivative of potential with x is zero). This position is called a virtual electrode.

By contrast, there is no visible formation of a virtual electrode when the barrier is as high as 0.3 eV and the MIM model is perfectly applicable in all operation regimes [Fig. 4(c)]. This is because the injected hole concentration is considerably lowered [by Eq. (3)] and the effect of "negative" electric field becomes negligible. From the comprehensive studies on the energy level alignment at metal/organic interfaces, it is found that Fermi level pinning appears in most material combinations, so the injection barrier cannot be lowered below a certain characteristic value.[23] In such a situation, perfect ohmic contact (zero injection barrier) cannot be achieved at any metal/organic interface and a barrier height of 0.3 eV is regarded as the most realistic one, so that the MIM picture is physically valid even under forward bias.

D. Forward-biased diode: Frequency-dependent impedance analysis

In conventional Si-based diodes, impedance analysis under forward-bias is not possible because the device becomes too conductive. Therefore, capacitance measurement is limited to the reverse-bias regime and the $1/C^2-V$ graph is often extrapolated into the forward-regime to gain information on the built-in potential of the diode. By contrast, pentacene-based diodes are more resistive, so that the impedance data in this regime can be analyzed through impedance spectroscopy over a broad frequency range (5 Hz to 2 MHz).

To avoid any misunderstanding, one should keep in mind that the existence of a depletion region under "forward-bias" cannot be in question. Even in the case of Schottky diodes, applying a forward bias cancels the energy barrier seen from the semiconductor toward the metal, and the depletion layer disappears as well. When the applied voltage exceeds V_{bi}, there is no more band banding or depletion region at the contact ("flatband condition" is fulfilled at the moment when V_a reaches V_{bi}). As a consequence, when one deals with the regime $V_a > V_{bi}$, there cannot be any depletion region. It is certain that in our cases, we did not observe any depletion region even under reverse-bias, and can neither see it under forward bias. Therefore, the applied voltage should distribute over the whole semiconductor thickness as shown in the band diagrams in Sec. III C.

Argand plot is the representation of impedance-frequency (Z-f) data on a complex plane, and it is useful to determine the equivalent circuit, since each circuit element responds differently to the frequency. The Argand representations of the data for the 515 nm diode [Fig. 5(a)] show perfect semicircles in the complex plane, which corresponds to the

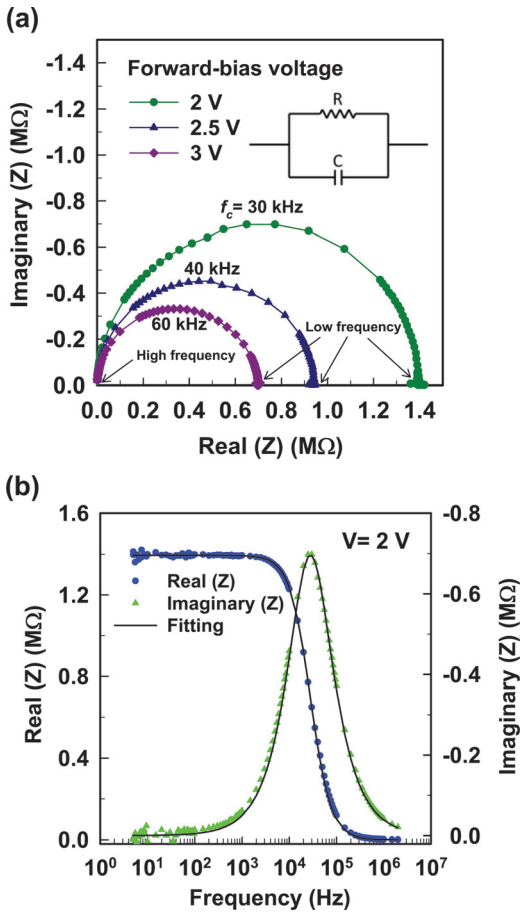

FIG. 5. (Color online) (a) Impedance-frequency (Z-f) data in the complex plane at different forward-bias voltages. The inset shows the equivalent circuit which corresponds to the shape of these curves. (b) Z-f plot with the fitting result using the parallel RC equivalent circuit.

response of a parallel resistance−capacitance (*RC*) circuit (see inset).[9,24]

The total (complex) impedance of a parallel *RC* circuit with given resistance (*R*) and capacitance (*C*) is expressed as[13]

$$Z = \frac{1}{\frac{1}{R} + j\omega C} = Z_{\mathrm{Re}} + jZ_{\mathrm{Im}}. \tag{4}$$

Z_{Re} is the real part of the total impedance and Z_{Im} is its imaginary part. Equations (4) can be reorganized to separate real and imaginary parts;

$$Z_{\mathrm{Re}} = \frac{R}{1+\omega^2R^2C^2}, Z_{\mathrm{Im}} = \frac{-\omega R^2C}{1+\omega^2R^2C^2}. \tag{5}$$

Two analyses are possible for obtaining separate *R* and *C* values from the *Z-f* data in the Argand plot. First, when $\omega \to 0$, Z_{Re} approaches *R* and Z_{Im} goes to zero according to Eq. (5). This means that the resistance *R* corresponds to the low-frequency intercept of the curve with Real (*Z*) axis [see Fig. 5(a)]. Next, the characteristic frequency ω_c at which Z_{Im} is minimum gives the *RC* time constant of the parallel *RC* circuit. By combining these two methods, *R* and *C* are independently accessible. In practice, ω_c is obtained by nullifying the first derivative of Z_{Im};

$$\left.\frac{dZ_{\mathrm{Im}}}{d\omega}\right|_{\omega=\omega_c} = 0 \quad \text{with} \quad \omega_c = 2\pi f_c = \frac{1}{RC}. \tag{6}$$

As shown by Eq. (6), the calculated value of ω_c (for the minimum Z_{Im}), is the reciprocal of *RC* time constant, and then f_c (in measurable "ordinary" frequency) is easily obtained. As one of the circuit parameters (namely, *R*) depends on the applied voltage (as will be shown in Fig. 6), f_c is also voltage-dependent as indicated on each curve in Fig. 5(a).

Z-f data were fitted to a simple parallel *RC* circuit using the software LEVM;[25] the results shown in Fig. 5(b) ensure the validity of the model. By comparison with other reports on the impedance analysis of organic diodes,[2,26,27] our data offer two distinctive features. First, we can neglect the contact resistance at the injecting contact (Au−pentacene interface), which often appears as a series element to the bulk circuit. The contact resistance might be negligibly small compared with the resistance of a thick, low mobility pentacene bulk film and the realization of a low-resistance, high-quality contact is attributed to the fact that the diode was entirely fabricated under a controlled oxygen-free ambient. Next, a single capacitance element is observed and can be directly related to the geometrical capacitance of the diode as defined by the overlapped area of two electrodes.

Both circuit parameters, resistance and capacitance, were extracted from the fitting process. Figure 6(a) shows the variation of the fitted resistance (red triangles) with V_a. The comparison of these values (from *Z-f* measurement) with the resistance estimated from the *I−V* measurement (dark blue circles) shows a very nice agreement. The bulk resistance decreases with V_a because of increasing injected charge density in the semiconductor. The variation of the extracted capacitance as a function of V_a is shown in Fig. 6(b). The capacitance is practically constant in the forward-bias regime, with a value slightly higher than that in the reverse-bias regime (3.77 pF) as calculated from *Z−V* measurements [Fig. 2(a)]. We attribute this small increase of the capacitance in the forward-bias regime to a small quantity of trapped charges inside the semiconductor bulk (no charges exist in the semiconductor bulk under reverse-bias). The increase of f_c with V_a [Fig. 5(a)] can be explained with the results in Fig. 6. With a constant *C* and decreasing *R*, the time constant *RC* also decreases and the corresponding f_c [Eq. (6)] is, as a result, an increasing function of V_a.

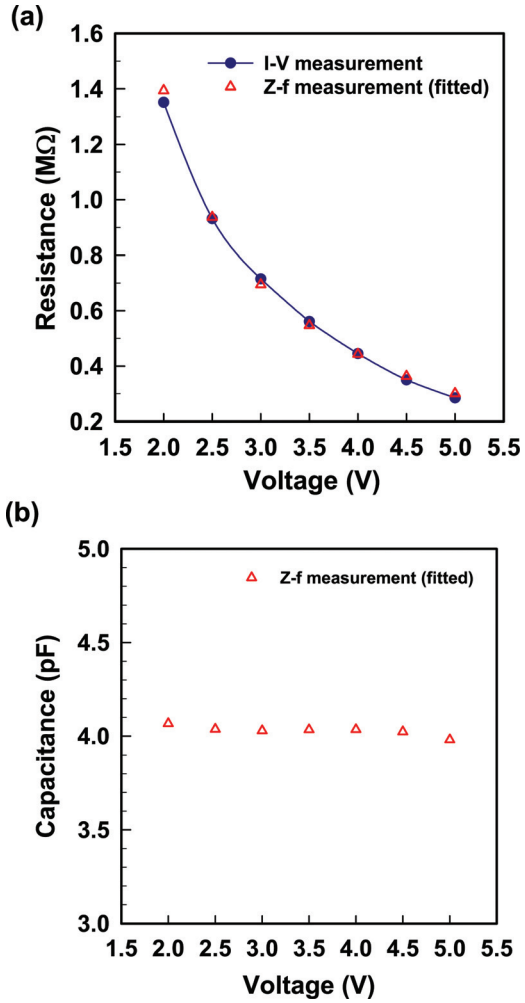

FIG. 6. (Color online) (a) Bulk resistance as a function of applied forward-bias. The circles show the resistances calculated from the first derivative of the *I−V* curve (Fig. 1) and the triangles represent the extracted parameters from the fitting of the *Z-f* measurements. (b) Fitted capacitance from the *Z-f* measurements.

E. Quasistatic dielectric constant of pentacene

Starting from the observation of a purely capacitive behavior of pentacene-based diodes in the reverse-bias regime, we could extract two important properties for characterizing any insulating materials; the dielectric constant (in this section) and the dielectric strength (in Sec. III F).

The dielectric constant of pentacene is often assumed to be around three based on optical determinations of the

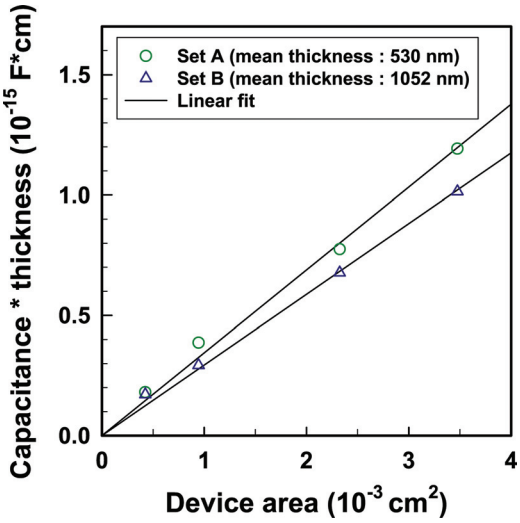

FIG. 7. (Color online) Extraction method of the dielectric constant of pentacene. Diodes with four different device areas are tested in each set. The measured geometrical capacitance and thickness are multiplied and plotted as a function of the device area. The slope of linear fits to the experimental results gives the average quasistatic dielectric constant multiplied by the permittivity of vacuum.

refractive indices.[20,28,29] The situation is similar for other less-studied organic semiconductors and many people take three as the dielectric constant without further experimental proof.[30–32] However, one cannot rely on this value for 'electrical' characterization because the dielectric constant is known to be frequency-dependent, so that its value in the quasistatic regime might substantially differ from that in the high-frequency, optical regime (higher than 10^{12} Hz).[33] It is clearly shown in Fig. 5(a) that within this frequency range (5 Hz to 2 MHz), the dielectric constant of pentacene is frequency-independent and the determination of dielectric constant from electrical measurements surely gives the "quasistatic" value. One can refer to Ref. 27, as an example, to understand how the frequency-dependent dielectric constant (dispersive characteristics) affects the results of an impedance spectroscopy.

Figure 7 suggests an extraction method of the quasistatic dielectric constant using the diode configuration. Diodes with four different contact areas have been measured to extract an average dielectric constant of the deposited films on two sets of devices. The reverse-bias $Z-V$ measurement gives a geometrical MIM capacitance and the thickness of the pentacene layer is precisely measured for each diode. Fringing-field effect at the side edges of the contact electrode on the capacitance can be neglected by taking into account the dimensions of the device, because the thickness is at most about 1 μm while the contacts have a rectangular shape with at least a few hundreds of μm length and width.[34] Figure 7 contains linear regressions (through the origin) to the data plotted as a function of the device area. From the simple equation of the parallel-plate capacitance

$$C = k\varepsilon_0 \frac{A}{d}, \tag{7}$$

where C is the capacitance, ε_0 the permittivity of vacuum, k the dielectric constant of the semiconductor, A the contact area and d the thickness of the semiconductor, the slope of the graph gives the dielectric constant multiplied by the permittivity of vacuum. The obtained quasistatic dielectric constant of pentacene is 3.89 ± 0.25 for Set A and 3.32 ± 0.17 for Set B.

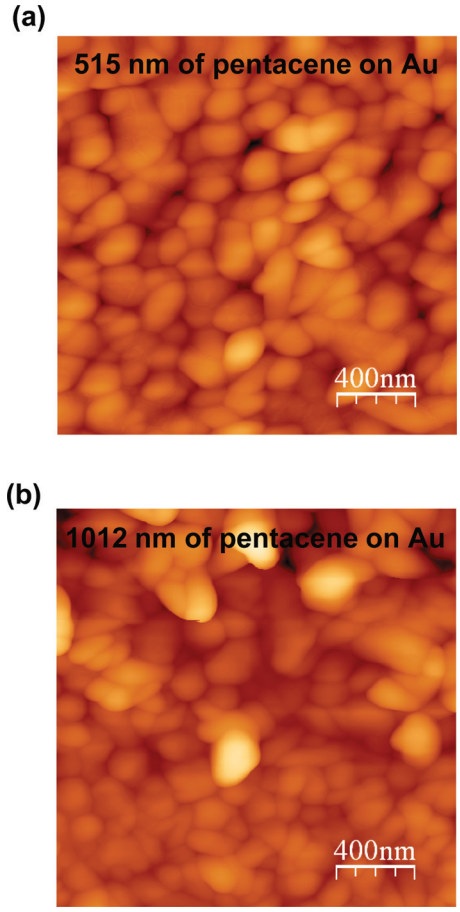

FIG. 8. (Color online) Tapping mode AFM images of pentacene layer on Au electrode (scan size: 2×2 μm^2); (a) 515 nm of pentacene, (b) 1012 nm of pentacene.

We do not believe that there is any significant effect of the film thickness on the dielectric constant because it is rather a "material" property of pentacene itself. The variation of the extracted dielectric constant in both sets of devices could be ascribed to the uncontrollable difference of the crystallinity of the films and/or the interface properties of the different diodes. Figure 8 presents the morphology of pentacene layers taken from each set of diodes. Both Figs. 8(a) and 8(b) are AFM images of the pentacene on Au electrode without Al top electrode (scan size: 2×2 μm^2). Figure 8(a) is taken for the diode with 515-nm pentacene (Set A) and Fig. 8(b) for the 1012-nm pentacene film (Set B). The polycrystalline structures of pentacene films are clearly shown in these images. Relatively small and nonuniform grains agree with previous works that reveal that pentacene deposition on Au generally results in flat-lying molecules and needlelike grains.[35,36] Even though the evaporation rate of pentacene and the substrate temperature were kept constant for both sets of devices, this accidental Au-pentacene interaction could give rise to the slight differences in crystallinity (Fig. 8) and dielectric constant (Fig. 7). In any case, one should

note that the dielectric constant is higher than the optical value, which is logical because with lower oscillation frequency, more polarization mechanisms can be involved and higher dielectric constant is expected.[33]

This electrical method could be applied to the delicate determination of the quasistatic dielectric constant of other organic semiconductors and could also help in understanding the variation of dielectric constant under various process/interface conditions.

F. Dielectric strength of pentacene

The dielectric strength of an insulating material is most often quantified by the measurement of the breakdown field (E_b), which is defined as the maximum electric field that can be applied before immediate breakdown.[37,38] This electrical breakdown causes, in generally, irreversible damages of the material due to the abnormally high current passing through it. In order to characterize the dielectric strength of pentacene (which has never been precisely quantified yet to our knowledge), 10 diodes were selected and reverse bias $I-V$ characteristics were measured until the breakdown occurred. The occurrence of electrical breakdown can also be seen by the optical microscopic images (Fig. 9) in which deterioration of electrodes and pentacene layer is apparently observable. In Fig. 10, the statistical average E_b of pentacene is

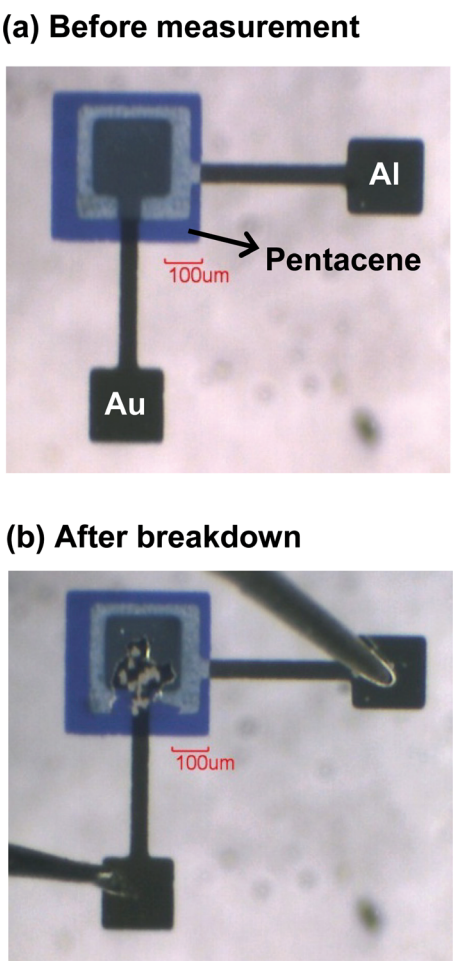

FIG. 9. (Color online) Optical microscopic images (a) before $I-V$ measurement and (b) after electrical breakdown due to high applied electric field.

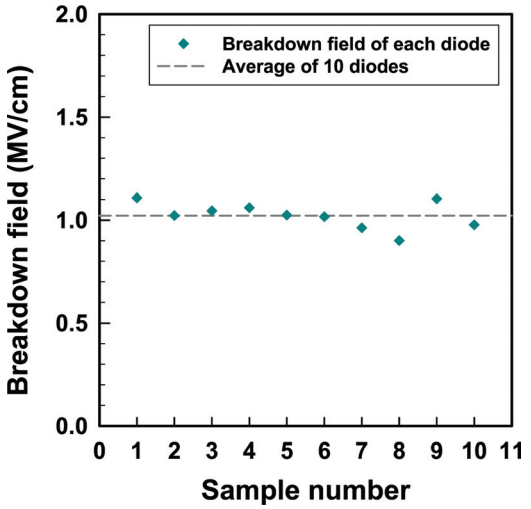

FIG. 10. (Color online) Scatter plot showing the variance of the measured E_b of pentacene in 10 diodes around the average value of 1.02 MV/cm.

calculated. From the 10 tested diodes, the dielectric strength is given as 1.02 ± 0.06 MV/cm. Compared with reported dielectric strength of well-known insulating materials, pentacene does not resist the application of high electric field. For example, thermally grown SiO_2 has E_b of 8–9 MV/cm and various polymeric insulators for OTFT application generally have E_b of 2–6 MV/cm.[37,38]

The relatively weak dielectric strength of pentacene (1.02 ± 0.06 MV/cm) can be attributed to several aspects. First possible cause is its polycrystalline morphology (Fig. 8) because a polycrystalline nature can easily result in the formation of pin holes and is known to have a weaker morphological stability against electrical stress compared to a disordered amorphous phase.[11] Second, the high-field region along the edges of the two electrodes could give rise to an early breakdown of the diode. It is known that this is the region where the electric field is significantly greater than the uniform field between the electrodes themselves and one can also find in Fig. 9(b) that the edge of the Al electrode offers a critical area for the occurrence of an electrical breakdown.

IV. CONCLUSION

In conclusion, the capacitive behavior of pentacene-based diode was investigated. Pentacene layers are fully depleted in the MSM configuration, which means that the current–voltage characteristics cannot be explained by the modulation of a Schottky barrier (modulation of the depletion region). Diode characteristics were then explained by MIM-type band diagram. Impedance analysis at all regimes shows a single capacitance element corresponding to the geometrical capacitance. A simple method for the extraction of the quasistatic dielectric constant of an organic semiconductor based on electrical measurements was suggested and the dielectric strength of pentacene was also quantified.

ACKNOWLEDGMENTS

This work has been supported by the NoE POLYNET from the European Community's Seventh Framework Program (FP7/2007-2013) under Grant No. 214006.

[1]T. Kaji, T. Takenobu, A. F. Morpurgo, and Y. Iwasa, Adv. Mater. **21**, 3689 (2009).
[2]D. Braga, M. Campione, A. Borghesi, and G. Horowitz, Adv. Mater. **22**, 424 (2010).
[3]D. M. Taylor and H. L. Gomes, J. Phys. D: Appl. Phys. **28**, 2554 (1995).
[4]P. Stallinga, H. L. Gomes, M. Murgia, and K. Müllen, Org. Electron. **3**, 43 (2002).
[5]A. Takshi, A. Dimopoulos, and J. D. Madden, Appl. Phys. Lett. **91**, 083513 (2007).
[6]S. M. Sze and K. K. Ng, *Physics of Semiconductor Devices*, 3rd ed. (Wiley, New York, 2007).
[7]S. Steudel, K. Myny, V. Arkhipov, C. Deibel, S. De vusser, J. Genoe, and P. Heremans, Nature Mater. **4**, 597 (2005).
[8]S. Steudel, S. De vusser, K. Myny, M. Lenes, J. Genoe, and P. Heremans, J. Appl. Phys. **99**, 114519 (2006).
[9]B. N. Pal, J. Sun, B. J. Jung, E. Choi, A. G. Andreou, and H. E. Katz, Adv. Mater. **20**, 1023 (2008).
[10]Y. S. Lee, J. H. Park, and J. S. Choi, Opt. Mater. **21**, 433 (2002).
[11]W. Brütting, S. Berleb, and A. G. Mückl, Org. Elecron. **2**, 1 (2001).
[12]O. D. Jurchescu, J. Baas, and T. T. M. Palstra, Appl. Phys. Lett. **87**, 052102 (2005).
[13]C. K. Alexander and M. N. O. Sadiku, *Fundamentals of Electric Circuits*, 2nd ed. (McGraw-Hill, New York, 2004).
[14]D. Braga, N. Battaglini, A. Yassar, G. Horowitz, M. Campione, A. Sassella, and A. Borghesi, Phys. Rev. B **77**, 115205 (2008).
[15]E. J. Lous, P. W. M. Blom, L. W. Molenkamp, and D. M. de Leeuw, Phys. Rev. B **51**, 17251 (1995).
[16]D. B. A. Rep, A. F. Morpurgo, and T. M. Klapwijk, Org. Electron. **4**, 201 (2003).
[17]A. Kahn, N. Koch, and W. Gao, J. Polym. Sci. Part B: Polym. Phys. **41**, 2529 (2003).
[18]F. Amy, C. Chan, and A. Kahn, Org. Electron. **6**, 85 (2005).
[19]R. Steyrleuthner, M. Schubert, F. Jaiser, J. C. Blakesley, Z. Chen, A. Facchetti, and D. Neher, Adv. Mater. **22**, 2799 (2010).
[20]Y. Zheng, A. T. S. Wee, C. Troadec, and N. Chandrasekhar, Appl. Phys. Lett. **95**, 143303 (2009).
[21]K. C. Kao and W. Hwang, *Electrical Transport in Solids with Particular Reference to Organic Semiconductors* (Pergamon, London, 1981).
[22]M. A. Lampert, J. Appl. Phys. **35**, 2971 (1964).
[23]S. Braun, W. R. Salaneck, and M. Fahlman, Adv. Mater. **21**, 1450 (2009).
[24]Y. Li, J. Gao, D. Wang, G. Yu, Y. Gao, and A. J. Heeger, Synth. Met. **97**, 191 (1998).
[25]J. R. Macdonald, CNLS (Complex Nonlinear Least Square) Immittance, Inversion, and Simulation Fitting Program, LEVMW version 8.08 (2007).
[26]V. S. Reddy, S. Das, S. K. Ray, and A. Dhar, J. Phys. D: Appl. Phys. **40**, 7687 (2007).
[27]C.-C. Chen, B.-C. Huang, M.-S. Lin, Y.-J. Lu, T.-Y. Cho, C.-H. Chang, K.-C. Tien, S.-H. Liu, T.-H. Ke, and C.-C. Wu, Org. Electron. **11**, 1901 (2010).
[28]O. D. Jurchescu, J. Baas, and T. T. M. Palstra, Appl. Phys. Lett. **84**, 3061 (2004).
[29]D. Faltermeier, B. Gompf, M. Dressel, A. K. Tripathi, and J. Pflaum, Phys. Rev. B **74**, 125416 (2006).
[30]A. Takshi, A. Dimopoulos, and J. D. Madden, IEEE Trans. Electron Devices **55**, 276 (2008).
[31]G. Liang, T. Cui, and K. Varahramyan, Solid-State Electron. **47**, 691 (2003).
[32]O. G. Reid, K. Munechika, and D. S. Ginger, Nano Lett. **8**, 1602 (2008).
[33]J. D. Livingston, *Electronic Properties of Engineering Materials* (Wiley, New York, 1999).
[34]W. C. Chew and J. A. Kong, IEEE Trans. Microwave Theory Tech. **28**, 98 (1980).
[35]G. Beernink, T. Strunskus, G. Witte, and Ch. Wöll, Appl. Phys. Lett. **85**, 398 (2004).
[36]C. Bock, D. V. Pham, U. Kunze, D. Käfer, G. Witte, and Ch. Wöll, J. Appl. Phys. **100**, 114517 (2006).
[37]A. Facchetti, M. -H. Yoon, and T. J. Marks, Adv. Mater. **17**, 1705 (2005).
[38]J. Melai, C. Salm, S. Smits, J. Visschers, and J. Schmitz, J. Micromech. Microeng. **19**, 065012 (2009).